# Thermal stability and oxidation resistance of Ti–Al–N coatings

Li Chen [a,b,*], Jörg Paulitsch [a], Yong Du [b], Paul H. Mayrhofer [a]

[a] *Department of Physical Metallurgy and Materials Testing, Montanuniversität Leoben, Leoben, 8700, Austria*
[b] *State Key Laboratory of Powder Metallurgy, Central South University, Changsha Hunan, 410083, China*

A B S T R A C T

$Ti_{1-x}Al_xN$ coatings are widely used for wear resistant applications due to their excellent mechanical and thermal properties, which depend to a great extent on the Al content. Here, we concentrate on a comparative study of the effect of Al content on crystal structure, thermal stability and oxidation resistance of $Ti_{1-x}Al_xN$ coatings. In agreement to earlier studies, thermal annealing of the individual cubic (c) and wurtzite (w) structured metastable $Ti_{1-x}Al_xN$ coatings induces decomposition into their stable phases c-TiN and w-AlN. The decomposition process for c-$Ti_{1-x}Al_xN$ involves an intermediate formation of cubic Al-rich and Ti-rich domains which results in a hardness increase to 34.7 and 34.4 GPa for $x = 0.52$ and 0.62 when annealed at 950 and 900 °C, respectively. In general, coatings with an Al content closer to the solubility limit, exhibit an earlier decomposition process, and hence an earlier peak-hardness.

During exposure of the $Ti_{1-x}Al_xN$ coatings to ambient air at elevated temperatures $Al_2O_3$, $TiO_2$ and $Al_2TiO_5$ are formed. The oxidation resistance of as-deposited single-phase $Ti_{1-x}Al_xN$ coatings, cubic or wurtzite structured, increases with increasing Al content. However, coatings containing Al contents at the metastable solubility limit, which result in a mixed cubic–wurtzite structure, have the worst oxidation resistance of the Al-containing coatings investigated. The single phase wurtzite structured coating w-$Ti_{0.25}Al_{0.75}N$ shows the best oxidation resistance, with only ~0.7 μm oxide scale thickness, after thermal exposure for 20 h at 850 °C in ambient air.

© 2011 Elsevier B.V. All rights reserved.

## 1. Introduction

Hard coatings are increasingly required for wear resistant applications on tools, dies, molds, and for components used in the automotive and aerospace industries, which always are exposed to severe tribological and thermal conditions. $Ti_{1-x}Al_xN$ coatings with cubic NaCl (c) structure, where Al substitutes for Ti in the TiN based structure (i.e., $Ti_{1-x}Al_xN$), is one of the most preferred material for such industrial applications due to the high hardness and wear resistance, combined with good thermal stability, oxidation resistance and the ability of age-hardening [1–7]. Especially the Al content within the $Ti_{1-x}Al_xN$ coatings plays an important role for their mechanical and thermal properties as well as their preferred crystal structure [1–5]. Single phase cubic $Ti_{1-x}Al_xN$ coatings with high Al contents exhibit excellent mechanical properties and oxidation resistance [1–5]. For Al contents exceeding the maximum solubility ($x_{max}$ ~0.7, depending on the depositions conditions used, see Ref. [8]) in the cubic phase, a mixed cubic-NaCl and wurtzite-ZnS (w) structure is formed. The wurtzite configuration exhibits lower hardness, bulk-, elastic-, and shear-moduli, as well as wear resistance [1–5].

Thermal stability and oxidation resistance of $Ti_{1-x}Al_xN$ coatings are the key factors of many important properties required for industrial applications [6–14]. When exposed to air at elevated temperatures, $Ti_{1-x}Al_xN$ coatings form a bilayer $Al_2O_3/TiO_2$ oxide scale, which strongly depends on the Al content [4]. According to the studies of Vaz et al. [4], the improved oxidation resistance is obtained with increasing Al content due to a reduced growth of the $TiO_2$ sub-layer oxide. However, the oxidation behavior deteriorates at critically high Al contents, where the transition from cubic to wurtzite structure takes place [4]. Thermal annealing of metastable $Ti_{1-x}Al_xN$ coatings results in the formation of their stable phases c-TiN and w-AlN [5–7]. Whereas detailed investigations are conducted for single phase cubic structured $Ti_{1-x}Al_xN$ coatings, which basically exhibit a spinodal decomposition process resulting in an increased hardness [5–7], only little is known for single phase wurtzite and mixed cubic–wurtzite structured coatings.

Consequently, to obtain a comparative investigation of the effect of Al content and the crystal structure on the thermal stability and oxidation resistance of $Ti_{1-x}Al_xN$ coatings, we prepared single-phase cubic TiN, $Ti_{0.48}Al_{0.52}N$ and $Ti_{0.38}Al_{0.62}N$, a mixed-phase (cubic and wurtzite) $Ti_{0.33}Al_{0.67}N$, and a single-phase wurtzite $Ti_{0.25}Al_{0.75}N$. These coatings are studied in detail with respect to their structure, mechanical and thermal properties. Annealing treatments in vacuum (up to 1500 °C) were conducted to investigate the changes in structure and hardness, whereas isothermal annealing treatments in

---

* Corresponding Author: Full mailing address: State Key Laboratory of Powder Metallurgy, Central South University 410083 Changsha Hunan China. Tel.: +86 731 888 36213; fax: +86 731 887 10855.
    E-mail address: chenli_927@126.com (L. Chen).

ambient air (at 850 °C for 20 and 40 h) were conducted to study the oxidation behavior as a function of Al-content and structure.

## 2. Experimental details

$Ti_{1-x}Al_xN$ coatings of various chemical compositions are developed by magnetically unbalanced magnetron sputtering of powder-metallurgically prepared Ti, $Ti_{0.5}Al_{0.5}$ and $Ti_{0.33}Al_{0.67}$ targets (diameter of 152.4 mm and purity of 99.9%, PLANSEE SE) in mixed $Ar + N_2$ (both of 99.999% purity) glow discharge. The chemical composition of the $Ti_{1-x}Al_xN$ coatings was further adjusted by adding Ti platelets (diameter of 5 mm and a thickness of 1 mm) on the sputtering race track of the $Ti_{0.5}Al_{0.5}$ target and using a $N_2$-partial pressure of either 17 (Ti and $Ti_{0.5}Al_{0.5}$ target) or 23% ($Ti_{0.5}Al_{0.5}$ and $Ti_{0.33}Al_{0.67}$ target). By varying the $N_2$-partial pressure and using a $Ti_{0.5}Al_{0.5}$ target, different chemical compositions in the resulting coatings are obtained. More details on the effect of deposition conditions on the chemical composition of the $Ti_{1-x}Al_xN$ coatings are described in Ref. [8]. The magnetron sputtering system used is described in Ref. [15]. The substrates were etched for 20 min using an $Ar^+$ glow discharge with −1250 V and 25 mA at a pressure of 3.0 Pa. The $Ti_{1-x}Al_xN$ coatings were prepared with a constant substrate temperature of 500 °C, 1.5 A magnetron power current, −60 V substrate bias potential, and 0.4 Pa working gas pressure. The base pressure of the chamber was always below 0.8 mPa. For the individual investigations, different substrates were used, see next paragraphs, which were cleaned in acetone and ethylene before placing them parallel above the target at a distance of 85 mm.

The chemical composition of as-deposited coatings (on austenitic stainless steel substrates, $20 \times 7 \times 2$ mm³) was determined using energy dispersive X-ray analysis (EDX) with an Oxford Instruments INCA EDS unit attached to a scanning electron microscope (SEM, Zeiss EVO 50) operated with 25 kV. Quantification of the elements was obtained by elemental standards and a TiN coating standard which has been quantified by Rutherford Back-scattering Spectroscopy. Nanoindentation measurements of as-deposited coatings and annealed coatings (20 min at annealing temperatures $T_a$ of 700, 800, 900, 950, 1000 and 1100 °C in vacuum (base pressure below 5 mPa) with a heating and cooling rate of 20 °C/min) on MgO (100) substrates ($10 \times 10 \times 1$ mm³) were conducted with a CSIRO ultra-microindentation system (UMIS) using a Berkovich indenter. With respect to a proper statistic, at least 30 indents were carried out for each sample with maximum loads ranging from 8 to 30 mN. Thereby the indentation depth was always below 7% of the coating thickness. Hardness and indentation moduli were calculated from the loading and unloading segments of the indentation curves using the Oliver and Pharr method [16]. Coated Si stripes ($20 \times 7 \times 0.3$ mm³, both sides polished) are used for residual stress measurements by the cantilever beam method.

Differential scanning calorimetry (DSC) with thermogravimetry (TGA) was performed in a calibrated Netzsch-STA 409C from room temperature (RT) to 1500 °C with a heating rate of 20 K/min in flowing He (99.999% purity, 20 sccm flow rate) and synthetic air (79% $N_2$, 21% $O_2$, 20 sccm flow rate) to mimic application conditions. He atmosphere was used instead of Ar or $N_2$ as it allows for a higher thermal conductivity and the possibility to investigate the N-release from the nitride coatings. The individual DSC curves were corrected using the re-measurement of the same material, immediately after the original measurement. Phase and structure changes of $Ti_{1-x}Al_xN$ coatings are determined by room-temperature X-ray diffraction (XRD) as a function of post-deposition annealing temperature $T_a$ (annealing in vacuum, base pressure below 5 mPa, heating and cooling rate of 20 °C/min) with a Bruker D8 in Bragg/Brentano mode and $CuK_\alpha$ radiation. For classification of XRD reflexes, the Powder Diffraction File database was used [17]. To avoid substrate interdiffusion and interference for these studies (DSC, TGA, and XRD), low alloy steel foil substrates were

used, which are removed by chemical etching with a 10 mol% nitric acid after the deposition, to have just freestanding coating materials. This procedure causes no detectable changes of the coating chemistry. The oxidation behavior of the coatings (on polycrystalline $Al_2O_3$ substrates, $20 \times 7 \times 0.5$ mm³) was studied by SEM fracture cross-sections after isothermal oxidation at 850 °C for 20 and 40 h in a Nabertherm N11/HR box-furnace.

## 3. Results and discussion

### 3.1. Structure and mechanical properties

Elemental analysis by EDX reveals that our $Ti_{1-x}Al_xN$ coatings are stoichiometric with N/metal ratios of $1 \pm 0.02$ for the $N_2$-partial pressures used. The obtained compositions are TiN, $Ti_{0.48}Al_{0.52}N$, $Ti_{0.38}Al_{0.62}N$, $Ti_{0.33}Al_{0.67}N$, and $Ti_{0.25}Al_{0.75}N$, and their thicknesses are 3.60, 4.24, 2.90, 2.69 and 3.08 µm, respectively. Fig. 1a presents XRD patterns of as-deposited freestanding (and powdered) $Ti_{1-x}Al_xN$ coatings. The coatings are single phase cubic structured for AlN mole fractions $x \leq 0.62$, mixed cubic and wurtzite structured for $x = 0.67$, and single phase wurtzite structured for $x \geq 0.75$. This is in
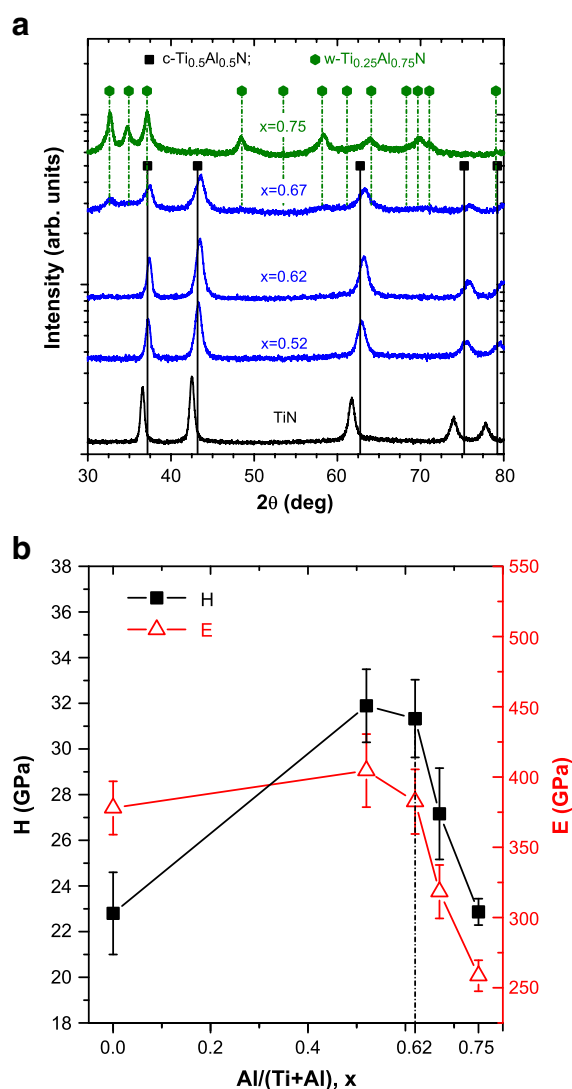
**Fig. 1.** (a) XRD powder scans of $Ti_{1-x}Al_xN$ coatings removed from their substrate and (b) hardness of $Ti_{1-x}Al_xN$ coatings on MgO (001) with Al contents x of 0, 0.52, 0.62, 0.67 and 0.75. The 2θ positions for c-$Ti_{0.5}Al_{0.5}N$ and w-$Ti_{0.25}Al_{0.75}N$ have been calculated using the cubic lattice parameter a = 4.185 Å and the wurtzite lattice parameter a = 3.169 Å with c/a = 1.62, according to Refs. [21,22].

excellent agreement with ab initio calculations suggesting that for x ~0.69 both phases, cubic and wurtzite, are equally favorable [18].

Hardness (H) and indentation modulus (E) of our $Ti_{1-x}Al_xN$ coatings as a function of Al content x are presented in Fig. 1b. With increasing Al content for the single phase cubic coatings the hardness increases from ~22.8 GPa for TiN to 31.9 GPa for $Ti_{0.48}Al_{0.52}N$ and 31.3 GPa for $Ti_{0.38}Al_{0.62}N$ due to changed binding characteristics. A further increase in Al content results in a decrease of H to ~27.2 GPa for $Ti_{0.33}Al_{0.67}N$ and further to ~22.9 GPa for $Ti_{0.25}Al_{0.75}N$ mainly due to the structural transformation from single phase cubic toward single phase wurtzite, respectively, compare Fig. 1a. This hardness dependence on the chemical composition and structure of the $Ti_{1-x}Al_xN$ coatings is in excellent agreement with earlier studies, see for example Ref. [19,20], and only slightly (below the error of measurement) influenced by different residual stresses of the coatings, which are −1.356, −1.446, −0.883, +0.102 and +0.186 GPa for TiN, $Ti_{0.48}Al_{0.52}N$, $Ti_{0.38}Al_{0.62}N$, $Ti_{0.33}Al_{0.67}N$, and $Ti_{0.25}Al_{0.75}N$, respectively. This transformation from compression to tension is connected with the structural transformation from single phase cubic toward mixed cubic and wurtzite to single phase wurtzite, compare Fig. 1a. The variation of the indentation moduli with the Al content for $Ti_{1-x}Al_xN$ follows the hardness variation, whereas the difference for E between c-TiN (E ~378 GPa) and c-$Ti_{0.48}Al_{0.52}N$ (E ~405 GPa) is not as pronounced as for H.

### 3.2. Thermal stability

Base line corrected dynamical differential scanning calorimetric (DSC) results of our $Ti_{1-x}Al_xN$ (x = 0, 0.52, 0.62, 0.67, and 0.75) coatings (Fig. 2a) indicate that several exothermic reactions occur during annealing in He-atmosphere to 1500 °C, according to the results presented in Ref. [6]. The TiN coating exhibits basically only a small exothermic output across the entire temperature range from 400 to 1500 °C. The exothermic signal increases for the as-deposited single phase cubic coatings with increasing Al content and then decreases again when the as-deposited coating structure changes toward single phase wurtzite. This corresponds to the stored energy (mixing enthalpy) within the individual metastable phases, as predicted by ab initio calculations see Refs. [18,21–24]. Furthermore, with increasing Al content x from 0.52 to 0.62 to 0.67 the first major exothermic peak temperature decreases from 800 to 670 to 600 °C, respectively.
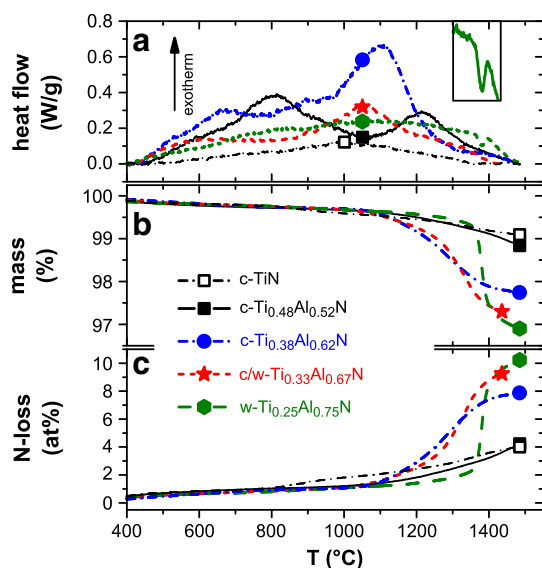
Correspondingly, the peak temperature of the second major exothermic peak shifts from 1220 °C for $Ti_{0.48}Al_{0.52}N$ to 1100 °C for $Ti_{0.38}Al_{0.62}N$ to 1050 °C for $Ti_{0.33}Al_{0.67}N$. The reduction in exothermic peak temperatures for the as-deposited single phase cubic coatings $Ti_{0.48}Al_{0.52}N$ and $Ti_{0.38}Al_{0.62}N$ is connected with an increase in exothermic signal and hence increased stored energy (mixing enthalpy), as also predicted by ab initio calculations. $Ti_{1-x}Al_xN$ with Al contents approaching the solubility limit (either cubic or wurtzite) exhibit an increased stored energy and hence an increasing driving force for decomposition [21]. The DSC signal of the c/w-$Ti_{0.33}Al_{0.67}N$ coating reflects the characteristics of the coatings c-$Ti_{0.38}Al_{0.62}N$ and w-$Ti_{0.25}Al_{0.75}N$. This is in excellent agreement with the structural investigations suggesting that the c/w-$Ti_{0.33}Al_{0.67}N$ coating is a combination of c-$Ti_{0.38}Al_{0.62}N$ and w-$Ti_{0.25}Al_{0.75}N$, see Fig. 1a.

The as-deposited single phase wurtzite structured w-$Ti_{0.25}Al_{0.75}N$ exhibits no distinct exothermic peak but an overall exothermic signal almost over the entire temperature range from 400 to 1500 °C, similar to c-TiN. Only at ~1350 °C there is the indication of a small endothermic reaction (see also the small inset in Fig. 2a), which is connected with a pronounced mass loss of ~3%, see Fig. 2b. Also for the other coatings a mass loss can be detected at $T_a \geq 1000$ °C, above their major exothermic reaction peaks, but over a wider temperature range, see Fig. 2b. Therefore, no endothermic feature can be detected during the DSC experiments of these coatings. Based on previous mass spectrometer studies, the mass loss can be attributed to N-release [25], which is presented in Fig. 2c as at.% of the individual $Ti_{1-x}Al_xN$ coatings. The data suggest that for c-TiN and c-$Ti_{0.48}Al_{0.52}N$ the N-release is similar and increases with increasing Al content.

Although a N-loss for c-TiN of 4 at.% and for w-$Ti_{0.25}Al_{0.75}N$ of even 10 at.% can be detected, both coatings exhibit an almost perfect match of their XRD patterns after annealing to $T_a = 1500$ °C with the standard peak positions of c-TiN and w-AlN [17], see Fig. 3a and b. The structural investigations after annealing at different temperatures are in good agreement with the simultaneous thermal analyses (Fig. 2) suggesting no major changes for c-TiN up to 1500 °C and w-$Ti_{0.25}Al_{0.75}N$ up to 850 °C. The XRD peaks of the c-TiN coating, Fig. 3a, gradually sharpen and move toward their standard positions with increasing annealing temperature, indicating structural changes toward a fully recrystallized stress-free material. The XRD peaks of
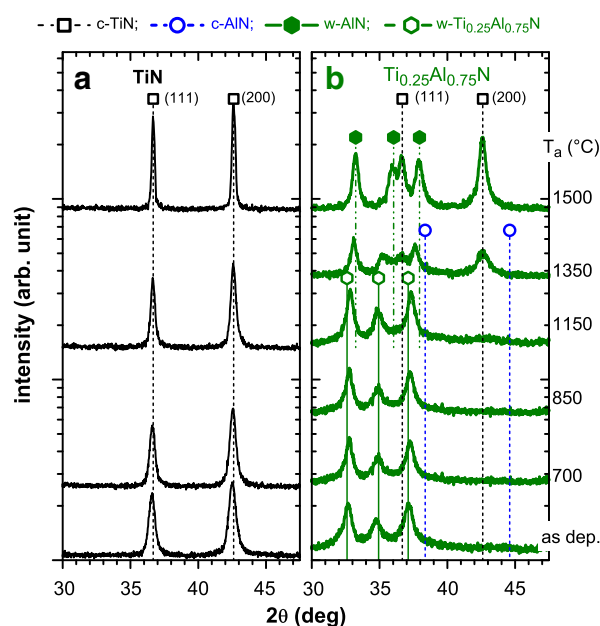


Fig. 2. Dynamical simultaneous thermal analysis combining (a) DSC and (b) TGA in inert atmosphere (He) of c-TiN, c-$Ti_{0.48}Al_{0.52}N$, c-$Ti_{0.38}Al_{0.62}N$, c/w-$Ti_{0.33}Al_{0.67}N$, and w-$Ti_{0.25}Al_{0.75}N$ freestanding coating materials. The inset in (a) is a section of the 4 times magnified DSC signal of w-$Ti_{0.25}Al_{0.75}N$ in the temperature range 1300–1425 °C. (c) Calculated N-release due to the measured mass-loss from (b).



Fig. 3. XRD powder scans of (a) c-TiN and (b) w-$Ti_{0.25}Al_{0.75}N$ coatings (removed from their substrates) after annealing in vacuum up to $T_a = 1500$ °C.

the w-$Ti_{0.25}Al_{0.75}N$ coating show a slight shift in position to higher diffraction angles during annealing to $T_a = 1150\,°C$ and indications for c-TiN formation. After annealing at $T_a = 1350\,°C$, where a pronounced mass loss (i.e., N-loss) occurs, c-TiN and w-AlN phase formation can clearly be detected. It is envisioned that the pronounced increase in large angle grain boundary fraction between the individual phases leads to a promoted $N_2$-release.

The structural investigations of the single phase cubic $Ti_{0.48}Al_{0.52}N$ and $Ti_{0.38}Al_{0.62}N$ coatings (Fig. 4a and b) reveal only a small shift of the XRD reflexes to higher diffraction angles during annealing to 700 °C, suggesting processes like recovery and stress-relaxation which contribute to the exothermic DSC feature in this temperature range. Furthermore, especially for the $Ti_{0.38}Al_{0.62}N$ coating a XRD peak broadening can be observed, which indicates a reduction in grain size and/or an increase in microstresses. Based on previous studies, these structural changes are due to isostructural decomposition to form cubic Ti-rich and Al-rich domains [18,21,25,26] via spinodal decomposition. The driving forces for this process are based on the increased total free energy when forming a supersaturated $Ti_{1-x}Al_xN$ crystal (with respect to their constituents TiN and AlN). This is described in more detail in Refs. [18,21–24] where also possible retarding forces for a decomposition process are discussed. The formation of cubic Ti-rich and Al-rich domains can better be seen after annealing at 950 °C, where on both sides (lower and higher diffraction angles) of the matrix XRD peak, shoulders are formed, which develop with increasing $T_a$ to 1100 °C, where also the formation of w-AlN can be detected. In agreement to the thermal analyses (Fig. 2) also the XRD data suggest a higher thermal stability for the lower Al-containing coating $Ti_{0.48}Al_{0.52}N$ as compared to $Ti_{0.38}Al_{0.62}N$. For $T_a = 1100\,°C$ still a major contribution of the as-deposited cubic solid-solution (matrix) can be detected for $Ti_{0.48}Al_{0.52}N$. Furthermore, for this coating (in contrast to $Ti_{0.38}Al_{0.62}N$) the metastable cubic Al-rich domain (at the XRD peak position of c-AlN) is clearly detectable up to $T_a = 1200\,°C$. The formation of w-AlN can be observed for both coatings at temperatures $T_a \geq 1100\,°C$ where also a pronounced mass loss (i.e., N-loss) occurs.

In agreement to the thermal analysis (Fig. 2) also the XRD data (Fig. 4c) show that the c/w-$Ti_{0.33}Al_{0.67}N$ coating is a combination of c-$Ti_{0.38}Al_{0.62}N$ and w-$Ti_{0.25}Al_{0.75}N$. Due to the structural changes also the hardness after annealing at different temperatures changes, as already shown in previous studies [6,7]. Here we want to highlight the

influence of the Al-content within an as-deposited single phase cubic structured coating (c-$Ti_{0.48}Al_{0.52}N$ and c-$Ti_{0.38}Al_{0.62}N$) and the difference to a dual phase (cubic and wurtzite) structured coating c/w-$Ti_{0.33}Al_{0.67}N$ and the single-phase wurtzite structured coating w-$Ti_{0.25}Al_{0.75}N$.

### 3.3. Age-hardening

The hardness of $Ti_{0.48}Al_{0.52}N$ is almost constant with values between 31.9 and 31.4 GPa upon annealing to 700 °C, see Fig. 5. In this temperature range, mainly recovery and relaxation processes occur (Fig. 4a), but spinodal decomposition can also be present as indicated by the exothermic output during DSC (which is larger as for TiN) and the results obtained for $Ti_{0.46}Al_{0.54}N$ in our earlier studies [27,28]. With a further increase in $T_a$, and hence further ongoing isostructural decomposition of the supersaturated cubic matrix (to form cubic Ti-rich and Al-rich domains), the hardness increases to ~34.7 GPa with $T_a = 950\,°C$. The formation of w-AlN and coarsening of the individual phases during annealing to 1100 °C leads to a significant decrease in H to ~27.3 GPa.

The higher Al-containing cubic c-$Ti_{0.38}Al_{0.62}N$ coating exhibits already a small increase in H from ~31.3 to 32.7 GPa with increasing $T_a$ to 700 °C. The more pronounced exothermic reaction in this temperature range (Fig. 2a), when compared with the lower Al-containing c-$Ti_{0.48}Al_{0.52}N$, suggests that for c-$Ti_{0.38}Al_{0.62}N$ the spinodal decomposition is already more developed, resulting in the small hardness increase. The maximum hardness of ~34.4 GPa is obtained for $T_a = 900\,°C$, before a noticeable w-AlN formation takes place. The advanced formation of w-AlN for higher annealing temperatures ($T_a > 950\,°C$, see Fig. 3c), leads to a decrease in hardness. The dual phase cubic and wurtzite coating c/w-$Ti_{0.33}Al_{0.67}N$ exhibits a comparable hardness evolution with $T_a$, but shifted to lower hardness values and temperatures. The peak-hardness of ~29.8 GPa is already obtained for $T_a = 800\,°C$. The single-phase wurtzite structured coating w-$Ti_{0.25}Al_{0.75}N$ exhibits the lowest hardness over the entire temperature range, but also a comparable hardness evolution. Although the XRD evolution with $T_a$ shows almost no change during annealing to 950 °C, it is envisioned that the wurtzite structured solid solution decomposes to form c-TiN precipitates already at 800 °C, resulting in the observed hardness increase to ~25.6 GPa. This is also based on the
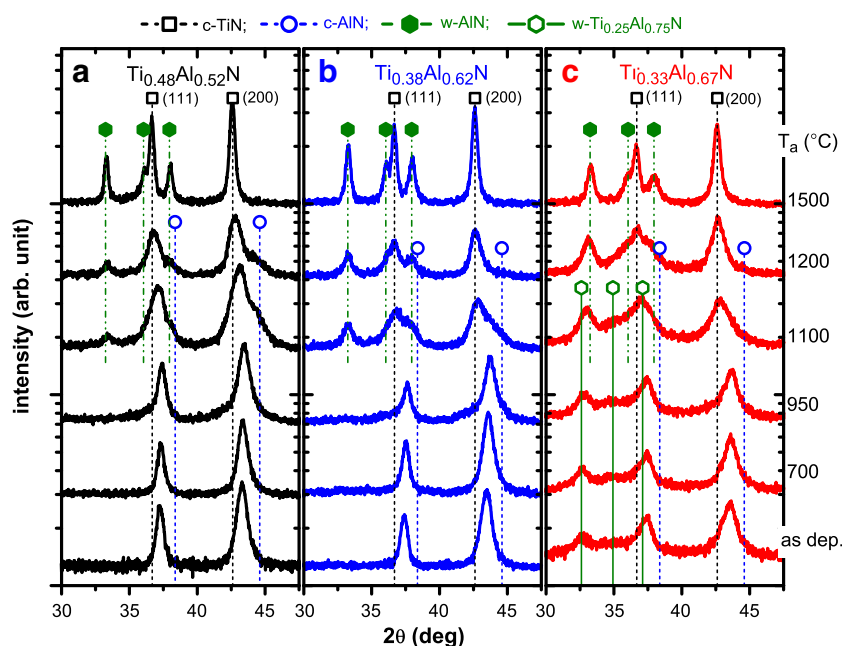


**Fig. 4.** XRD powder scans of (a) c-$Ti_{0.48}Al_{0.52}N$, (b) c-$Ti_{0.38}Al_{0.62}N$, and (c) c/w-$Ti_{0.33}Al_{0.67}N$ coatings (removed from their substrates) after annealing in vacuum up to $T_a = 1500\,°C$.
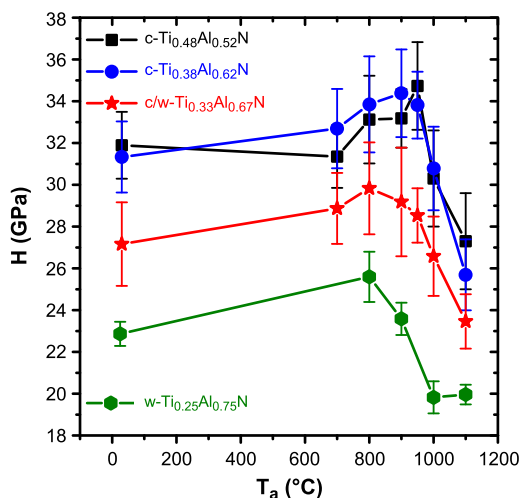
**Fig. 5.** Hardness, H, of $Ti_{1-x}Al_xN$ layers on MgO (001) after annealing in vacuum for 20 min at $T_a$.

DSC measurements, indicating an exothermic output in this temperature range. Further increasing the temperature to 1100 °C causes the hardness to decrease to 20.0 GPa.

The observed H vs. $T_a$ curves for our $Ti_{1-x}Al_xN$ coatings are in excellent agreement to the performed thermal analyses and structural investigations. The peak-hardness is obtained at temperatures slightly below the second major exothermic DSC feature (Fig. 2a) and before a noticeable w-AlN formation is present (Fig. 4). Generally, we can confirm, that a higher Al content within the cubic structure favors spinodal decomposition (hence earlier increase in hardness with $T_a$) due to an increase in driving force (mixing enthalpy), as suggested by ab initio calculations, see Refs. [18,21–24].

### 3.4. Oxidation resistance

Fig. 6 shows dynamic DSC experiments of powdered $Ti_{1-x}Al_xN$ freestanding coating samples up to 1450 °C in synthetic air. All Al-containing coatings investigated here exhibit an onset of the pronounced exothermic peak due to oxidation at ≥800 °C, hence, at least ~300 °C above that for c-TiN. The DSC data further show that the single phase cubic coating with the highest Al content (c-$Ti_{0.38}Al_{0.62}N$) as well as the single phase wurtzite coating (w-$Ti_{0.25}Al_{0.75}N$) exhibit the

highest onset (~900 °C) and peak temperature (~1000 °C) for the pronounced oxidation reaction. Noticeable also is that the dual-phase (cubic and wurtzite) coating c/w-$Ti_{0.33}Al_{0.67}N$ shows a ~100 °C lower onset temperature for the pronounced oxidation reaction as the other Al-containing coatings. The endothermic reaction at ~1350 °C, independent on the chemical composition, is due to sintering processes of the powdered samples.

XRD investigations of the $Ti_{1-x}Al_xN$ coatings after the DSC measurement to 1450 °C show a complete transformation to $TiO_2$, $Al_2TiO_5$ and $\alpha$-$Al_2O_3$, see Fig. 7. The data suggest that the phase fraction of $TiO_2$ decreases and that of $\alpha$-$Al_2O_3$ increases with increasing Al-content and that $Al_2TiO_5$ is the major phase for the Al-containing coatings.

Based on the DSC investigations (Fig. 6) we have chosen 850 °C for further isothermal oxidation studies of our Al-containing coatings. SEM fracture cross sections of the coatings on polycrystalline $Al_2O_3$ substrates after 20 h at 850 °C reveal oxide layer thicknesses of ~1.7, 1.1, 1.5 and 0.7 μm for Al contents of x = 0.52, 0.62, 0.67, and 0.75, respectively (Fig. 8a, b, c and d). Especially the low Al-containing single phase cubic c-$Ti_{0.48}Al_{0.52}N$ and the dual-phase c/w-$Ti_{0.33}Al_{0.67}N$ coatings exhibit a porous nature of their oxide scale at the interface to the remaining nitride coating (Fig. 8a and c). This porous layer is Ti-rich, whereas the more dense top-layer is Al-rich as proven by EDX measurements. This is in agreement with previous studies suggesting that the oxide scale of $Ti_{1-x}Al_xN$ coatings grows by simultaneous outward diffusion of Al toward the oxide/air interface and inward diffusion of O to the oxide/nitride interface where Ti is oxidized [4]. The formation of a dense $Al_2O_3$ top-layer retards the inward diffusion of O during oxidation of $Ti_{1-x}Al_xN$ coating, and is beneficial to their oxidation resistance. Additionally, the formation of a porous $TiO_2$ sub-layer is connected with the generation of compressive stresses [4], which can lead to crack formation within the oxide scale [4], as observed also during our studies, see Fig. 8a. The high Al-containing single phase wurtzite coating w-$Ti_{0.25}Al_{0.75}N$ exhibits a dense oxide scale with an almost homogeneous element distribution across the 0.9 μm scale thickness. Further oxidation at 850 °C for 40 h causes a complete oxidation of the coatings with Al contents of x = 0.52, 0.62 and 0.67, see Fig. 9a, b, and c. Contrary, the single-phase wurtzite w-$Ti_{0.25}Al_{0.75}N$ coating is still intact underneath a homogenous, dense and thin oxide layer of ~1.1 μm, see Fig. 9d. After thermal exposure in ambient air for 20 h at 950 °C all coatings are fully oxidized.
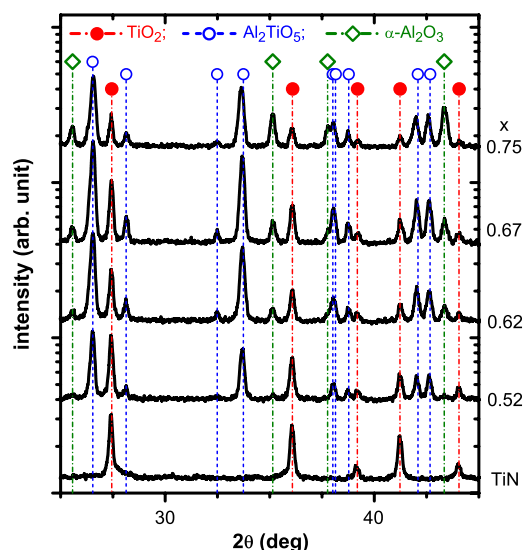


**Fig. 6.** DSC analysis in synthetic air of $Ti_{1-x}Al_xN$ with Al contents of x = 0, 0.52, 0.62, 0.67 and 0.75.



**Fig. 7.** XRD patterns of powdered $Ti_{1-x}Al_xN$ coatings after DSC in synthetic air to 1450 °C.
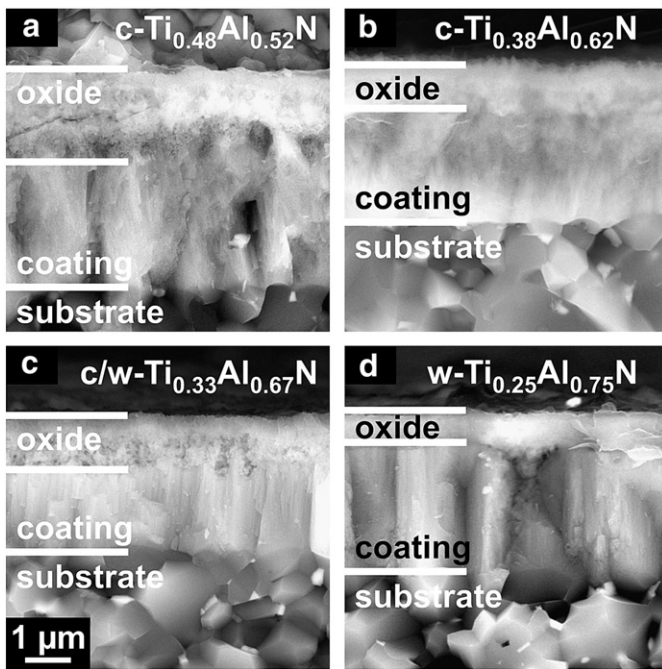
**Fig. 8.** SEM fracture cross section images of (a) c-Ti$_{0.48}$Al$_{0.52}$N, (b) c-Ti$_{0.38}$Al$_{0.62}$N, (c) c/w-Ti$_{0.33}$Al$_{0.67}$N, and (d) w-Ti$_{0.25}$Al$_{0.75}$N coatings on polycrystalline Al$_2$O$_3$ after isothermal oxidation at 850 °C for 20 h.

## 4. Conclusions

In this work we studied the structure, mechanical and thermal properties of magnetron sputtered Ti$_{1-x}$Al$_x$N coatings with varying Al content. The structural investigations indicate that Ti$_{1-x}$Al$_x$N is single phase cubic for AlN mole fractions x ≤ 0.62, mixed cubic and wurtzite for x = 0.67, and single phase wurtzite for x ≥ 0.75. The obtained hardness values of ~22.8 GPa for TiN, 31.9 GPa for Ti$_{0.48}$Al$_{0.52}$N, 31.3 GPa for Ti$_{0.38}$Al$_{0.62}$N, ~27.2 GPa for Ti$_{0.33}$Al$_{0.67}$N



**Fig. 9.** SEM fracture cross section images of (a) c-Ti$_{0.48}$Al$_{0.52}$N, (b) c-Ti$_{0.38}$Al$_{0.62}$N, (c) c/w-Ti$_{0.33}$Al$_{0.67}$N, and (d) w-Ti$_{0.25}$Al$_{0.75}$N coatings on polycrystalline Al$_2$O$_3$ after isothermal oxidation at 850 °C for 40 h.

and 22.9 GPa for Ti$_{0.25}$Al$_{0.75}$N strongly scale with the Al content and structure.

Thermal annealing of metastable Ti$_{1-x}$Al$_x$N coatings causes a structural transformation toward their stable constituents of c-TiN and w-AlN. For single-phase cubic coatings, this transformation is induced by an isostructural formation of cubic Ti-rich and Al-rich domains leading to an increased hardness. The decomposition toward the stable constituents is promoted for coatings having an Al content close to the solubility limit, as thereby their stored energy and hence the driving force increases. Hence, especially the Ti$_{0.33}$Al$_{0.67}$N coating, which consists of co-existing cubic and wurtzite phases already in the as-deposited state, exhibits the earliest onset of decomposition toward the stable phases c-TiN and w-AlN. Consequently, this coating shows also the earliest decline in hardness vs. temperature.

Whereas annealing treatments in vacuum showed the most promising results for c-Ti$_{0.48}$Al$_{0.52}$N (highest peak hardness of 34.7 GPa at the highest temperature of T$_a$ = 950 °C), the oxidation studies exhibit the highest onset temperature for pronounced oxidation for the higher Al containing coating c-Ti$_{0.38}$Al$_{0.62}$N. After oxidation of 20 h at 850 °C, this coating exhibits the thinnest oxide scale of ~1.1 μm among the cubic structured coatings. Only the single phase wurtzite structure coating w-Ti$_{0.25}$Al$_{0.75}$N shows a better oxidation resistance with ~0.7 μm oxide scale thickness, which only slightly increases to 1.1 μm by increasing the oxidation time at 850 °C to 40 h, where all other coatings tested here are completely oxidized.

## References

[1] K. Knutsson, M.P. Johansson, L. Karlsson, M. Oden, Surf. Coat. Technol. 205 (2011) 4005.
[2] S. PalDey, S.C. Deevi, Mater. Sci. Eng., A 342 (2003) 58.
[3] D. McIntyre, J.E. Greene, G. Hakansson, J.-E. Sundgren, W.-D. Münz, J. Appl. Phys. 67 (3) (1990) 1542.
[4] F. Vaz, L. Rebouta, M. Andritschky, M.F. da Silva, J.C. Soares, J. Eur. Ceram. Soc. 17 (1997) 1971.
[5] A. Hörling, L. Hultman, M. Oden, J. Sjölen, L. Karlsson, Surf. Coat. Technol. 191 (2005) 384.
[6] P.H. Mayrhofer, A. Hörling, L. Karlsson, J. Sjölen, T. Larsson, C. Mitterer, L. Hultman, Appl. Phys. Lett. 83 (2003) 2049.
[7] R.M. Saoubi, H. Chandrasekaran, Mach. Tools Manuf. 44 (2004) 213.
[8] L. Chen, M. Moser, Y. Du, P.H. Mayrhofer, Thin Solid Films 517 (24) (2009) 6635.
[9] P.H. Mayrhofer, C. Mitterer, H. Clemens, L. Hultman, Prog. Mater. Sci. 51 (2006) 1032.
[10] A. Raveh, I. Zukerman, R. Shneck, R. Avni, I. Fried, Surf. Coat. Technol. 201 (2007) 6136.
[11] A. Knutsson, M.P. Johansson, L. Karlsson, M. Oden, J. Appl. Phys. 108 (2010) 044312.
[12] L. Hultman, Vacuum 57 (2000) 1.
[13] J. Patscheider, T. Zehnder, M. Diserens, Surf. Coat. Technol. 146–147 (2001) 201.
[14] F. Rovere, P.H. Mayrhofer, A. Reinholdt, J. Mayer, J.M. Schneider, Surf. Coat. Technol. 202 (2008) 5870.
[15] P.H. Mayrhofer, M. Geier, C. Löcker, L. Chen, Int. J. Mater. Res. 8 (2009) 1052.
[16] W.C. Oliver, G.M. Pharr, J. Mater. Res. 7 (1992) 1564.
[17] International Center for Diffraction Data, PDF-2/Release 2007, card numbers 25-1133 (w-AlN), 38-1420 (c-TiN), 25-1495 (c-AlN), 21-1276 (TiO2), 46-1212 (Al2O3), 41-0258 (Al2TiO5).
[18] P.H. Mayrhofer, D. Music, J.M. Schneider, J. Appl. Phys. 100 (2006) 094906.
[19] A. Kimura, H. Hasegawa, K. Yamada, T. Suzuki, Surf. Coat. Technol. 120 (1999) 438.
[20] H. Hasegawa, A. Kimura, T. Suzuki, Surf. Coat. Technol. 132 (2000) 76.
[21] P.H. Mayrhofer, F.D. Fischer, H.J. Böhm, C. Mitterer, J.M. Schneider, Acta Mater. 55 (4) (2007) 1441.
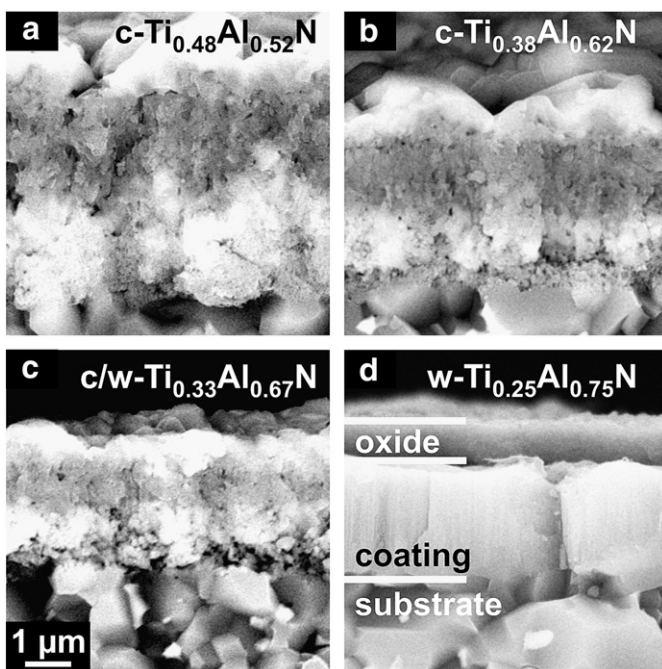[22] D. Holec, R. Franz, P.H. Mayrhofer, C. Mitterer, J. Phys. D: Appl. Phys. 43 (2010) 145403.

[23] B. Alling, A.V. Ruban, A. Karimi, O.E. Peil, S.I. Simark, L. Hultman, I.A. Abrikosov, Phys. Rev. B 75 (2007) 045123.
[24] R.F. Zhang, S. Veprek, Mater. Sci. Eng., A 448 (2007) 111.
[25] M. Moser, P.H. Mayrhofer, Materials 3 (3) (2010) 1573.
[26] F. Adibi, I. Petrov, L. Hulman, U. Wahlström, T. Shimizu, D. McIntyre, J.E. Greene, J.-E. Sundgren, J. Appl. Phys. 69 (1991) 6437.
[27] R. Rachbauer, S. Massl, E. Stergar, D. Holec, D. Kiener, J. Keckes, J. Patscheider, M. Stiefel, H. Leitner, P.H. Mayrhofer, J. Appl. Phys. 110 (2011) 023515.
[28] R. Rachbauer, E. Stergar, S. Massl, M. Moser, P.H. Mayrhofer, Scr. Mater. 61 (7) (2009) 725.